AD-A062 932 UNIVERSITY OF MANCHESTER INST OF SCIENCE AND TECHNOLO--ETC F/G 20/5
SYSTEMS FOR STUDY OF PROPAGATION OF CO2 LASER RADIATIONS THROUG--ETC(U)
OCT 78 P F BROWNE, P M WEBBER DA-ERO-77-G-060

UNCLASSIFIED NL

1 OF 1
AD
A062932

END
DATE
FILMED
3--79
DDC

SYSTEMS FOR STUDY OF PROPAGATION OF CO_2 LASER RADIATIONS THROUGH CLOUDS

by

P.F. Browne and P.M. Webber

October, 1978.

EUROPEAN RESEARCH OFFICE
United States Army
London, England

DAERO-77-G-060

University of Manchester Institute of Science and Technology,
Manchester M60 1QD, England.

Approved for public release; distribution unlimited.

SECURITY CLASSIFICATION OF THIS PAGE (When Data Entered)

REPORT DOCUMENTATION PAGE

READ INSTRUCTIONS BEFORE COMPLETING FORM

1. REPORT NUMBER

2. GOVT ACCESSION NO.

3. RECIPIENT'S CATALOG NUMBER

4. TITLE (and Subtitle)

SYSTEMS FOR STUDY OF PROPAGATION OF CO_2 LASER RADIATIONS THROUGH CLOUDS.

5. TYPE OF REPORT & PERIOD COVERED

FINAL TECHNICAL REPORT. MAY 77 - OCT 78,

6. PERFORMING ORG. REPORT NUMBER

7. AUTHOR(s)

P. F./BROWNE
P. M./WEBBER.

8. CONTRACT OR GRANT NUMBER(s)

DAERO-77-G-060

9. PERFORMING ORGANIZATION NAME AND ADDRESS

10. PROGRAM ELEMENT, PROJECT, TASK AREA & WORK UNIT NUMBERS

6.11.02A/1T161102BH57-01-00
655

11. CONTROLLING OFFICE NAME AND ADDRESS

UNIVERSITY OF MANCHESTER INSTITUTE OF SCIENCE AND TECHNOLOGY, MANCHESTER, U.K.

12. REPORT DATE

OCTOBER 1978

13. NUMBER OF PAGES

30

14. MONITORING AGENCY NAME & ADDRESS(if different from Controlling Office)

U.S. ARMY R&S GP (EUR)
BOX 65, FPO NEW YORK 09510

32p.

15. SECURITY CLASS. (of this report)

UNCLASSIFIED

15a. DECLASSIFICATION/DOWNGRADING SCHEDULE

16. DISTRIBUTION STATEMENT (of this Report)

APPROVED FOR PUBLIC RELEASE; DISTRIBUTION UNLIMITED

17. DISTRIBUTION STATEMENT (of the abstract entered in Block 20, if different from Report)

18. SUPPLEMENTARY NOTES

19. KEY WORDS (Continue on reverse side if necessary and identify by block number)

INFRARED SCATTERING, INFRARED ATTENUATION, LASER, AEROSOL ABSORPTION, CLOUD PHYSICS.

20. ABSTRACT (Continue on reverse side if necessary and identify by block number)

This report describes the design, and progress toward the construction, of systems required for the study of the propagation of 10.6 μm radiation from CO_2 lasers (both high power pulsed and cw) through clouds, both laboratory generated and natural. The laboratory experiments of highest priority are the study of non-linear attenuation of high power TEA laser pulses (of order 10 J/cm^2) through optically thick clouds produced by adiabatic expansion with

CONT. OVERLEAF

DD FORM 1 JAN 73 1473 EDITION OF 1 NOV 65 IS OBSOLETE

UNCLASSIFIED

SECURITY CLASSIFICATION OF THIS PAGE (When Data Entered)

particular attention to change of pulse shape, and measurements of backscatter The systems required for these experiments are nearing completion. The field experiments are the study of attenuation, beam quality and backscatter of TEA laser pulses and cw radiation over a return path of the order of 1 km. The systems required are under consturction. All lasers and also the transmissometer have been developed within the group.

SYSTEMS FOR STUDY OF PROPAGATION OF CO_2 LASER RADIATIONS THROUGH CLOUDS

by

P.F. Browne and P.M. Webber

October, 1978.

EUROPEAN RESEARCH OFFICE
United States Army
London, England

DAERO-77-G-060

University of Manchester Institute of Science and Technology,
Manchester M60 1QD, England.

ABSTRACT

This report describes the design, and progress toward the construction, of systems required for the study of the propagation of 10.6 μm radiation from CO_2 lasers (both high power pulsed and cw) through clouds, both laboratory generated and natural. The laboratory experiments of highest priority are the study of non-linear attenuation of high power TEA laser pulses (of order 10 J/cm^2) through optically thick clouds produced by adiabatic expansion with particular attention to change of pulse shape, and measurements of backscatter. The systems required for these experiments are nearing completion. The field experiments are the study of attenuation, beam quality and backscatter of TEA laser pulses and cw radiation over a return path of the order of 1 km . The systems required are under construction All lasers and also the transmissometer have been developed within the group.

CONTENTS

1. Introduction

The period from May, 1977 to October, 1978 has been spent in developing equipment which is necessary in order to carry out our proposed study of the propagation of 10.6 μm radiations from CO_2 lasers through clouds, both laboratory-generated and natural. Both high power pulses from a TEA laser and 30W cw beams from a conventional low pressure diffusion-cooled CO_2 laser will be used. These lasers have been developed within the group. The proposed research is an extension of work carried out under a previous contract (DAJA 37-74-C-1686, 1976).

In this report only the systems which are required in order to carry out the proposed experiments will be described. Most of this development work was carried out under the previous contract, but there was a need to improve and reengineer the laser systems and also the cloud chamber. This work has now been completed. A transmissometer for field measurements, and a portable repetitively pulsed (and possibly sealed off) TEA laser have been designed and are under construction.

2. Summary of Previous Work

Investigations of the attenuation of high power CO_2 TEA laser pulses by laboratory clouds were reported previously [1]. The main results in this work were as follows.

The TEA laser, which possessed novel features described elsewhere [2], had parameters listed in Table 1 . It delivered pulses of energy 20J and duration 0.1 μs with a beam diameter of 5 to 6 cm. The energy per unit beam area, about 1 J/cm^2 , was below the theoretical threshold for non-linear propagation, namely 2.75 J/cm^2 . The 200 MW pulses were detected by a photon drag detector with voltage responsivity 0.18 mV/kW and sensitive area 4 mm x 4 mm . Two such detectors, one for the attenuated beam and one for the reference beam which passed around the cloud chamber, were connected directly to the inputs of a double beam oscilloscope; this procedure was necessary in order to minimize the electrical pick-up associated with the laser discharges.

TABLE 1: Photoionization TEA Laser Parameters

Discharge dimensions	6 cm x 6 cm x 45 cm
Discharge volume	1.6 litre
Electrode separation	6 cm
Charging voltage	90 kV
Electric Field	15 kV/cm
Storage capacitance	0.06 μF @ 90 kV or 2 x 1.12 μF @ 45 kV
Energy discharged	240 J
Output energy	24 J (efficiency 10%)
Pulse duration	0.1 μs
Peak pulse power	240 MW
Beam diameter	$\approx$5 cm
Beam area	20 cm^2
Preionization	2 lines of 34 arcs fed by 0.5 μF capacitor @ 45 kV
Optical cavity	uncoated Ge etalon (72% reflectivity) Cu-Zr:Au 7.5 cm mirror with+3 m radius of curvature
Cavity length	105 cm
Beam divergence	10 mrad (multimode)

Clouds were produced in the laboratory by adiabatic cooling of air with high relative humidity in a large glass chamber of diameter 0.5 m and length 1.5 m (volume 250 litre). Gas from a commercially available cylinder of compressed air was fed into the cloud chamber with ports P_1 and P_2 closed and also the solenoid venting valve closed (see figure 1). Usually the input gas was fed through an electrical discharge in order to provide ions as nuclei for condensation. The pressure in the chamber was allowed to build up to 5 or 6 psi above atmospheric pressure (14.7 psi). Sudden venting by opening the 1" solenoid valve lowered the temperature uniformly throughout the chamber in the manner shown in the chart recordings of figure 2 . During pressurization the gas in the chamber heated several degrees, but if allowed to stand radiation cooling brought the temperature back to room temperature in a few minutes. On venting the chamber the temperature fell by typically 11 °C for 5 psi excess pressure and 13.5 °C for 6 psi excess pressure. These figures depended on the relative humidity due to release of latent heat during condensation. Figure 4 shows the temperature falls from 300 °K to be expected theoretically for various excess pressures in the case of (i) dry air and (ii) saturated air. For example, if Δp = 6 psi then a temperature fall of 28 °C is expected for dry air, but only 6.7 °C for saturated air. From the observed temperature fall one may infer the initial relative humidity.

Let compressed gas at initial temperature T_1 and relative humidity h suffer a temperature fall to T_2' on expansion from pressure p_1 to p_2. Had the gas been dry, the calculated final temperature is T_2 , where

$$T_2/T_1 = (p_2/p_1)^{0.286} \qquad (1)$$

Then the latent heat liberated during condensation of mass $\Delta\rho$ per unit volume, namely $L\Delta\rho$, must equal the heat acquired by the gas when its temperature rises from T_2 to T_2' presumably at constant volume, so that

$$L\Delta\rho = \rho_a c_v (T_2' - T_2) \qquad (2)$$

where L (= 2257 J grm^{-1}) is the latent heat , ρ_a is the mass of gas per unit volume (= 1.293 x 10^{-3} grm cm^{-3}) and c_v is the specific heat at constant volume for air (= 0.718 J grm^{-1} K^{-1}). Thus

$$\Delta\rho = 0.41(T_2' - T_2) \text{ grm m}^{-3} \qquad (3)$$

Since the gas at the final temperature is saturated and contains water vapour per unit volume $\rho_s(T_2')$ which can be read off the graph of figure 3 , we know that the amount of water vapour initially present was $\rho_s(T_2') + \Delta\rho$. The initial relative humidity can then be calculated from:

$$h = [\rho_s(T_2') + \Delta\rho]/\rho_s(T_1) \qquad (4)$$

The values for a typical case are shown in table 2. It should be noted

TABLE 2: Calculation of water condensed and initial humidity

Excess pressure (Δp)	6 psi
Initial temperature (T_1)	300 °K
Observed temperature fall ($T_1 - T'_2$)	13.5 °K
Temperature fall for dry air ($T_1 - T_2$)	28.0 °K
Water condensed ($\Delta\rho$)	5.5 grm m^{-3}
Relative humidity initially (h)	67.8 %

that values of $\Delta\rho$ and h are higher if c_p rather than c_v is appropriate in (2) since c_p = 1.006 J grm^{-1} K^{-1}.

Generally our clouds last only about 5 minutes before evaporating. Calculation shows that this is due to radiant heating, not convection and of course not conduction. If the final temperature of the cloud is equal to or above room temperature the cloud lasts much longer, and we have produced clouds with lifetimes up to an hour. Ultimately descent of the

drops under Stokes's law limits the lifetime of the cloud. The velocity of descent decreases as the square of the radius (see figure 5). Thus a drop of radius 1.5 μm (typical of our clouds) requires about 17 minutes to decend a distance of 25 cm, half the diameter of the tube.

At visible wavelengths the clouds produced with ion nucleation are quite opaque, even when viewed transversely. At the wavelength of the He-Ne laser the attenuation over a 1.5 m path exceeds 30 dB. An attenuation of 20 dB/m , or 20,000 dB/km , is very much greater than is observed for natural clouds, for example at Great Dun Fell in Cumbria where Sanders and Selby [3] measured attenuations at 0.63 μm in the range 50 - 400 dB/km .

At wavelength 10.6 μm the laboratory clouds reduced the beam intensity by a factor of about 2 over the 1.5 m path, which corresponds to about 2 dB/m or an extinction coefficient γ_{ext} of 0.46 m^{-1}:

$$\gamma_{ext} = z^{-1} \ln[I(z)/I(0)] = 0.46 \ m^{-1} \qquad (5)$$

From relation (A9) of the appendix we can relate the linear absorption coefficient γ to the mass of water condensed in unit volume $\Delta\rho$:

$$\gamma_{ext} = \gamma + \gamma_s \qquad \gamma = 0.112 \Delta\rho \ m^{-1} \qquad (\Delta\rho \text{ in grm/m}^3) \qquad (6)$$

Substituting $\gamma = 0.46 \ m^{-1}$, one infers $\Delta\rho = 4.1$ grm/m^3 . This agrees with the values calculated from (3), so that it is probably valid to neglect γ_s in comparison with γ . The neglect of γ_s means that the drops were of small size - see, for example, the relative contributions of absorption and scattering to attenuation as a function of radius in calculations quoted in reference [12]. The measurement of backscatterin gives a direct value for γ_s by use of relation (A21) of the appendix.

Let N(a)da be the concentration of drops with radii in $a \rightarrow a + da$. From equations (A3), (A4) and (A8) of the appendix, we see that the cross section for absorption by a water drop of radius a is $n_w \gamma_w V$ where $V = 4\pi a^3/3$:

$$\gamma = \int \sigma(a) N(a) \, da \qquad \sigma(a) = n_w \gamma_w (4\pi a^3/3) \qquad (7a)$$

It is assumed that the drop is optically thin, which means $2a < 10\mu$m for wavelength 10.6 μm . The attenuation of 0.63 μm radiation, on the other hand, is due mainly to scattering, and the cross section for scattering is $\pi a^2 K(a)$ where the factor K(a) has to be calculated from Mie theory:

$$\gamma_s = \int \sigma_s(a) N(a) da \qquad \sigma_s(a) = \pi a^2 K(a) \qquad (7b)$$

Hence, if the cloud is monodisperse or nearly so, we can find the drop radius a from

$$a = \frac{3K}{2\gamma_w n_w} \frac{\gamma(10.6)}{\gamma_s(10.63)} \simeq 15.8 \frac{\gamma(10.6)}{\gamma_s(10.63)} \ \mu m \qquad (8)$$

If we assume K(a) = 2, which is the value to which K approaches as ak $\gg$ 1 , then the observed values $\gamma(10.6) = 0.46 \ m^{-1}$ and $\gamma_s(0.63) = 4.6 \ m^{-1}$ (i.e. 30 dB attenuation over 1.5 m path) lead to $a = 1.58 \mu$m . The drop concentration then follows from $VN = \Delta\rho$. To summarize:

$$a = 1.58 \ \mu m \qquad N = 3 \times 10^5 \ cm^{-3} \qquad (9)$$

The drops are therefore smaller than those of typical natural clouds (see figure 13). The assumption that the cloud is approximately monodisperse is probably justified, in view of the results obtained by Cole et al. [4] for clouds produced in the same way. Moreover, on occasion it was possible to see visually the descent under Stokes's law of a well defined cloud ceiling.

3. Modifications to Equipment

(i) Cloud Chamber:

In a number of respects the cloud chamber needed improvement. The most obvious was a completely rigid structure on which to mount it, and more importantly, the ancillary optics for deflecting the beams as shown in figure 1 . Ultimately the pick-up problem may be overcome by use of slow response detectors for pulse energy (though not, of course, profile). In view of the excessive cost of commercial volume absorbing calorimeters for detection of TEA laser pulses, it is planned to devise our own such detectors; since only a ratio of two pulse energies is important for attenuation measurements, the problem of absolute calibration of the device will not arise. The photon drag detectors previously used are required if pulse shape is to be examined; however, in order to see a signal superimposed on the pick-up it was necessary to focus the pulses onto these detectors which then operated near the threshold for damage, and in any case presented only a small area with which to sample the beam. A completely rigid framework has now been made of $1\frac{1}{2}$ inch square ste l tube, and is bolted to the floor. See figure 12 .

Although the clouds, when initially produced, were optically deep even at 10.6 μm, it is desirable to have a considerably longer path length. In order to be able to pass a beam through the chamber a number of times by multiple reflections, the ports P_1 and P_2 were widened to 6 inch diameter. This created a new problem in sealing the chamber for pressures up to 1.5 atm. by port doors which could be opened and closed by remote control and which opened outwards. This was solved ingeniously by use of pneumatic rams, two for each port. One ram opens and closes the port door, and the other seals it against the large outward force when pressurized as shown in figure 1 inset.

In order to increase the lifetime of our clouds it was necessary to arrange that the final temperature after adiabatic expansion is above room temperature. This requires preheating of the pressurized gas by some 15 ^{o}C or so. With this aim in view, and also in order to increase the initial humidity, an electric kettle heater element has been incorporated so as to heat the water in the bottom of the tube. There also is provision for a liquid nitrogen heat exchanger at the top of the chamber in order to establish a temperature gradient from bottom to top of the chamber and so generate clouds convectively.

A mistake that was made during the initial alterations was to orientate the chamber vertically. Such orientation would be interesting for hole burning by the cw CO_2 laser since convection would not tend to draw further drops into the beam. However, it was found that when the ports P_1 and P_2 were opened the cloud rushed out of the top or the bottom port depending on whether the final temperature was above or below room temperature. This convective flow, of course, was much faster than Stoke's law descent. Only by use of internal mirrors could this be prevented; the appropriate port would remain closed with a mirror on the inside which would return the beam, but the mirror would require to be heated in order to prevent surface condensation. It was decided to orientate the chamber horizontally again, and gain the advantage of no mirrors or windows.

(ii) High Energy TEA Laser

The high energy TEA laser, whose development and performance was reported elsewhere [2] , required a certain amount of reengineering quite apart from any improvements.

In order to be able to operate at less than atmospheric pressure

without oxygen contamination the laser was incorporated into a gas-tight glass chamber 12 inches in diameter with 1 inch thick perspex end flanges to which reflectors are mounted. The circuitry was fitted into a much smaller oil bath with a great reduction in weight, and increased use of strip transmission line reduced circuit inductance which is always desirable in order to reduce the risk of arcs rather than uniform discharges.

The aim in developing this laser is to propagate through our laboratory clouds TEA laser pulses whose energy per unit beam area exceeds the threshold for non-linear attenuation, 2.73 J cm^{-2} . In its original form the TEA laser delivered 20 J pulses multimode with beam diameter 5 cm and angular divergence 10 mrad.; this corresponds to about 1 J cm^{-2} . Over a distance of 1.5 m the divergence is such as to spread the beam by 1.5 cm . In order to reduce the beam divergence an unstable resonator of the type employed by Dyer et al. [5] will be incorporated. Dyer et al. achieved beam divergence of only 0.2 mrad. by use of an unstable resonator consisting of a convex mirror (diameter 7.5 cm) with radius of curvature 29 m and a plane mirror (diameter 2.85 cm) at distance 1.3 m from the convex mirror; this is the diffraction limit for an aperture of diameter 6.25 cm . In order to increase the energy per unit area of beam, one requires a beam reducer. This will increase the divergence by a factor M , where M is the magnification of the reducer as a telescope. If one could achieve a divergence comparable with the diffraction limit for a 2 inch aperture, namely 0.25 mrad. , then beam reduction from 5 cm diameter to 1 cm diameter would increase the divergence to only 1.25 mrad. which is acceptable for the experiment. The energy per unit beam area would increase to some 20 J cm^{-2} , assuming the same pulse energy from the unstable resonator. With these considerations in mind, and thinking also of ease of alignment of the optics, it has been decided to incorporate the beam reducer into the laser cavity as shown in figure 6 .

4. Transmissometer for TEA and CW CO_2 Lasers

With the aim of equiping a van as a mobile unit for transmission studies of various types of natural precipitate, a number of systems have been designed and at present are under construction. The main systems are (i) a portable repetitively pulsed and possibly sealed-off CO_2 TEA laser, (ii) a 30 W CW CO_2 TEA laser, (iii) a transmit-receive telescope of Cassegrain type, (iv) a corner-cube retroreflector, and (v) detection equipment with protection against pick-up . Because of workshop and other facilities, such a transmissometer would have to be built and serviced at the UMIST laboratories, so that the purchase and equiping of a van is essential for studies in the field. Trial tests will be made between the roof of the physics laboratories and nearby tall buildings at ranges of perhaps 500 m . Some details of these systems are now presented.

(i) Portable Repetitively Pulsed CO_2 TEA Laser:

A small portable repetitively pulsed CO_2 TEA laser which may be sealed-off (unless this proves too difficult) has been designed and now is being constructed (figures 7 &11). A double-discharge type of TEA laser is particularly suitable for a field instrument. Since preionization is achieved by a corona-type discharge to tungsten wires which are capacitively coupled to one main electrode rather than by an array of arcs, only one high voltage charging circuit is required. Because there is no blinding flash from the arc array the uniformity of the main discharge can be checked visually rather than by looking for air-breakdown. Interelectrode spacing will

be small enough to permit operation without voltage doubling, which effects a further simplification of the circuit. Our high rate capacitor charging unit (Hartley Measurements model 401) has a maximum of 60 kV (the charging current varies with the state of charge, and the absence of charging resistors permits rapid charging without power dissipation). The design parameters for this TEA laser are listed in Table 3 .

TABLE 3: Design Parameters for Double-Discharge TEA Laser

Discharge dimensions	3.5 cm x 3.5 cm x 40 cm
Discharge volume	0.49 litre
Electrode separation	3.5 cm
Charging voltage	55 kV
Electric field	16 kV/cm
Storage capacitance	0.01 μF
Energy discharged	15 J
Output energy	1.5 J
Pulse duration	0.1 μs
Peak pulse power	15 MW
Beam diameter	2.5 cm
Beam area	5 cm^2
Preionization	corona discharge to W wires
Optical cavity	uncoated Ge etalon (1.5" diam. 72% refl.) Cu-Ni: Au convex mirror (1.5" diam., ~30 m radius of curvature)
Cavity length	80 cm
Beam divergence	0.5 mrad (diffraction limit for 2.5 cm)

In the device reported by Stark et al. [6] sealed-off operation was achieved by addition of small quantities of CO and H_2 in order to promote the reverse reaction in the equilibrium, $CO_2 \rightleftharpoons CO + O$. Gibson et al. [7] achieve sealed-off operation by circulating the laser gas mix over a catalyst bed at room temperature (60% MnO_2, 40% CuO) and by using as seed gas trimethylamine $(CH_3)_3N$ with ionization potential 7.82 eV . Sealed-off operation is an obvious advantage for a field instrument, and it will be attempted.

(ii) CW CO_2 Laser :

What was a crudely constructed CW laser of conventional diffusion-cooled design has been completely redesigned and reconstructed, and now is ready for testing (figures 8 and 11). A discharge at about 15 torr of laser gas mix is run in two pyrex glass tubes of diameter 0.7 cm, each 70 cm long. Between the tubes is a central anode which is water cooled and which serves also as a gas outlet. At their other ends the tubes couple directly to metal T sections used as cathodes and gas inlets. The cathodes are independently ballasted by 180 kΩ high dissipation resistors. If the central anode is earth the T sections will run at up to 10 kV above earth potential, so that the small glass end sections which support Brewster angle ZnSe windows then float at high potential. The external reflectors, however, are earthed to the aluminium alloy channel base which provides a rigid base for their mountings. These reflectors can then be adjusted during operation of the laser. A glass cooling jacket is integral with each discharge tube. Coupling of the tube to the metal electrodes is accomplished by commercial O-ring units shown in the inset to figure 8 . The parameters for this laser, as judged from those of a similar laser constructed at SERL, Baldock, are shown in Table 4.

TABLE 4: Parameters of CW CO_2 Laser

Diameter of discharge tube	0.7 cm
Length of discharge	2 x 70 cm = 140 cm
Ballast resistance	180 kΩ
Discharge current	2 x 20 mA = 40 mA
Cathode voltage (anode earth)	9 kV
Power dissipated	360 W
Cooling	by diffusion to walls (water cooled)
Efficiency	14 %
Output power (multimode)	50 W
Output power (single mode)	10 W (selected by 4 mm aperture in cavity)
Gas mix	CO_2: 8.3% , N_2: 16.6%, He 75.1%
Flow rate	4 gas changes per second
Optical cavity	Cu-Ni:Au concave mirror, 20 m radius of c. Ge flat, 85% coating on inside, AR coating on outside
Cavity length	192 cm
Beam diameter	4 mm
Beam divergence	1.7 mrad.

(iii) Transmit-Receive Cassegrain Telescope:

It is planned to use the same telescope to transmit and to receive the beam after reflection by a 'cats-eye' or 'corner-cube' retroreflector. This eliminates the problem of two-way communication for one-way transmission measurements, although it may create a problem of pick-up in detector circuitry. However, backscatter measurements will be provided for.

For a 1 km range the optics must be designed for minimum beam divergence. The TEA laser described in section 4(i) will have a beam of diameter 2.5 cm and divergence about 0.5 mrad. provided that an unstable resonator is incorporated as shown in figure 7 . The unstable resonator will be of the type used by Dyer et al. [5] as described in connection with the high energy TEA laser (section 3ii); 0.5 mrad. is the diffraction limit for aperture 2.5 cm. If the Cassegrain telescope has magnification 10 then the transmitted beam will have diameter 25 cm and beam divergence 0.05 mrad. The spread of the beam over a path of 2 km is then only 10 cm , and a corner-cube reflector with dimensions of the order of 25 cm (1 ft) will return most of the transmitted power. With regard to the CW CO_2 laser , the divergence of 1.7 mrad mentioned in Table 4 is appropriate for diffraction by an aperture of diameter 0.7 cm. Preliminary beam expansion by a factor of about 4 may be necessary before feeding into the Cassegrain transmitting telescope. See reference 8 .

(iv) Corner-Cube Retroreflector

A corner-cube retroreflector is now under construction. Purchase of an ex-service stock of front-aluminized optically flat glass plates of dimensions 6" x 6" was made some time ago with this end in view. Three such flats mounted to metal backing plates will have independent screw adjustment with respect to a rigid corner cube mounting structure. Protection from rain and a demisting arrangement will be required.

(v) Detection

Since only a ratio of pulse energies or of CW intensities is required for attenuation measurements, the problem of absolute calibration of a detector is avoided. For high powers photon drag detectors offer the advantage of speed of response, and are essential for pulse profile measurements. Our photon drag detectors have responsivity 0.2 mV/kW and sensitive area 4 mm x 4 mm. Pyroelectric detectors, although thermal in principle, have fast response (because their internal impedance is capacitive

the stray capacitance at the input of an amplifier does not cause loss of signal at high frequencies. Our TGS pyroelectric crystal (sensitive area 2 mm x 2 mm) with FET amplifier (Plessey model PSC 222) has voltage responsivity of 10^{-2} V/W with a maximum of 1 mW on the sensitive area (for model PPC 222 the maximum is 1 W).

The problem of pick-up is best overcome by time delay. Over 1 km range the transit time is about 3.3 μs . Thermal delay in the detector itself also should be effective.

The construction of a large aperture detector, for example of the type reported by Stricker and Rom [9] may be most suitable for the ratio of pulse energy measurements involved in a transmissometer.

The CW laser lends itself to heterodyne detection of very weak return signals, for example those due to backscatter in the atmosphere. A pyroelectric detector with normal minimum detectable signal of 3×10^{-9} W (due to noise) can typically detect 2.5×10^{-15} W for local oscillator power of only 1 mW. Hughes et al. [10] were able to range noncooperative reflecting objects such as trees up to 10 km away, and they obtained measurable backscatter from aerosols in the atmosphere.

5. Planned Experiments

(i) Laboratory Cloud Measurements:

The main aim with regard to the laboratory produced clouds is to study the propagation of TEA laser pulses with high energy per unit beam area W - specifically, with values of W exceeding the threshold for the explosive evaporation of droplets, 2.73 J/cm^2 . The modified optics for the high energy TEA laser described in section 3(ii) might yield $W \simeq 20$ J/cm^2 .

The threshold represents the condition that sufficient energy should be absorbed from the pulse of 10.6 μm radiation by a drop in order to first heat the drop to boiling point (requiring 334 J/grm) and then evaporate the drop (requiring the latent heat of 2257 J/grm). For drops with diameter less than about 10 μm the rate of absorption of energy is proportional to the volume of the drop, as is also the heat required for evaporation, and hence the condition is independent of drop size. If one imagines the drop distorted into the shape of a cylinder with base area A and height Δz such that $A\Delta z = V$ where V is the drop volume then the energy absorbed in time dt is $\gamma_w IA\Delta z dt$ where I is the intensity of the 10.6 μm beam and γ_w is the linear absorption coefficient for liquid water (951 cm^{-1} at 10.6 μm wavelength). Hence

$$-\eta(H + L)d(dV) = \gamma_w IA\Delta z dt = \gamma_w IV dt \qquad (9)$$

where H is the energy to boil unit mass of water, L is the latent heat of evaporation, d is the density of water, and dV is the volume evaporated in time dt . η is a factor to take into account loss of heat to surroundings. For TEA laser pulses the heating is so quick that we may take $\eta \simeq 1$. However

Mullaney et al. [11] inferred that $\eta \simeq 3$ for a CW CO_2 laser with $5 < I < 50$ W. Writing (9) in the form,

$$dV/dt = -V/\tau \qquad \tau = \eta d(H + L)/(\gamma_w I) \tag{10}$$

one finds that the drop volume V or the drop radius a decrease with time t in accordance with

$$V(t) = V(0)\exp(-t/\tau) \qquad a(t) = a(0)\exp(-t/3\tau) \tag{11}$$

where

$$I\tau = \eta d(H + L)/\gamma_w = 2.73\eta \quad J/cm^2 \tag{12}$$

However, TEA lasers can deliver the energy required for eventual evaporation of a drop in a time less than that required for physical expansion of the water vapour. By focussing TEA laser pulses on single drops Kafalas and Ferdinand [12] studied this expansion. For a drop of radius 12μm a spherical front of water vapour expanded at 130 m/s over the first 1.3 μs (eventually at 15 m/s). For optically thick drops a dumbbell type of expansion occurred due to front surface evaporation and rear surface spallation on arrival of a shock from the front surface. The expanding shock fronts were further studied by Kafalas and Herrmann [13]. Our TEA laser pulses have duration 0.1 μs, in which time the vapour front can expand a distance of 13 μm which is about equal to the radius of the original drop. Of course we have the same number of water molecules in about one eighth the original volume, and so the transition from the water phase to the vapour phase occurs in a time comparable with the pulse duration. Thus the strong absorption of the liquid phase, due to hydrogen bonding, must give way to the weak absorption of water vapour before the pulse has entirely passed over the drop. Presumably this should be visible as a change of pulse shape. Thus the study of pulse shape above the threshold for non-linear propagation is high on the agenda.

The measurement of backscattering from the laboratory clouds as depicted in figure 9 should be a sensitive indicator of drop radius since the backscattered signal will be proportional to NV^2, and hence to a^3 for constant water content. Also, one may infer the scattering coefficient γ_s (see appendix).

(ii) Natural Precipitates:

It is planned to measure attenuation of 10.6 μm radiation by natural precipitates in a variety of atmospheric conditions. Both TEA laser pulses and CW radiations will be investigated.

Another propagation parameter which it is planned to measure is beam quality, which is defined as the fraction of laser power which is collected by an area of radius $\lambda f/D$, where f is the focal length of the mirror or lense used to intercept the beam and D is the diameter of the laser aperture (were the laser aperture uniformly illuminated, then $1.22\lambda/D$ would be the diffraction spread of the beam) or the width of a Gaussian beam.

The transmissometer is well adapted for measuring backscatter. This is a useful measurement because of the information it provides about the precipitate (see appendix).

APPENDIX A: COMPLEX REFRACTIVE INDEX

Let a medium have a complex refractive index $\tilde{n}$ and put

$$\tilde{n} = n + in' \tag{A1}$$

Then the electric field of a plane electromagnetic wave which propagates in the z-direction through the medium is given by

$$E = E_o e^{i(\tilde{n}kz - \omega t)} = E_o e^{-n'kz} e^{i(nkz - \omega t)} \tag{A2}$$

Thus the intensity I ($\propto E^2$) decreases with z in accordance with

$$I(z) = I(0)e^{-\gamma z} \qquad \gamma = 2n'k \tag{A3}$$

We can always relate complex refractive index to a complex electric susceptibility for the medium $\tilde{\chi}$ by

$$\underline{D} = \underline{E} + 4\pi\underline{P} \qquad \tilde{n}^2 = \epsilon = 1 + 4\pi\tilde{\chi} \tag{A3}$$

Here $\underline{D}$ is electric displacement and $\underline{P}$ is the polarization (dipole moment per unit volume). Writing $\tilde{\chi} = \chi + i\chi'$, we then have

$$\begin{aligned} n^2 - 1 - n'^2 &= 4\pi\chi \\ 2nn' &= 4\pi\chi' \end{aligned} \tag{A4}$$

The dipole moment per unit volume of medium is $4\pi\tilde{\chi}E$. We shall neglect polarization induced by the field of the dipoles themselves, so that no Lorentz-Lorentz term will arise in our expression for $\tilde{n}$; this is justified because the mean separation of drops is greater than the wavelength λ. It remains to relate $\tilde{\chi}$ to the dipole moments of individual water drops, assumed to be small compared to λ.

(I) Small Drops ($ak \ll 1$)

When drop radius a is much less than λ, so that $ak \ll 1$, there is no diffraction or specular reflections at the surface of the drops to consider. The induced polarization of the drops is much the same as for single molecules or atoms. Let $N(a)da$ be the concentration of drops with radii in $a \to a + da$. Then, if $\tilde{\chi}_w$ is the electric susceptibility of liquid water at the radiation frequency, the dipole moment of a drop is $\tilde{\chi}_w VE$ where $V = (4\pi/3)a^3$, and the dipole moment per unit volume is

$$P = 4\pi\int(4\pi a^3/3)\tilde{\chi}_w E N(a)da = 4\pi\tilde{\chi}E \tag{A5}$$

Hence

$$\tilde{\chi} = (4\pi/3)\int a^3 N(a)da\,\tilde{\chi}_w = (\Delta\rho/d)\tilde{\chi}_w \tag{A6}$$

In the same way as $\tilde{\chi}$ is related to $\tilde{n}$ we can relate $\tilde{\chi}_w$ to $\tilde{n}_w$, which at 10.6 μm wavelength has the value [14]

$$n_w = 1.175 + (0.0802)i \tag{A7}$$

Hence

$$\begin{aligned} \gamma_w &= 2n_w'k = 951\ \text{cm}^{-1} \\ \gamma &= 2n'k = (\Delta\rho/d)\gamma_w(n_w/n) \end{aligned} \tag{A8}$$

where we use (A3) and (A4). If γ is measured in m^{-1} and $\Delta\rho$ in grm/m^3, then the second relation of (A8) becomes

$$\boxed{\gamma = 0.112\,\Delta\rho} \tag{A9}$$

(II) Large Drops ($ak \geq 1$)

Above, the scattering particles (whether atoms or drops) have been treated as dipole oscillators. Each dipole of the medium is the source of a secondary Huygen-type spherical wavelet, and these secondary wavelets interfere in such a manner as to produce a resultant secondary wave with the same geometry as the incident wave. Let the dipole moment of a scattering particle be $\underline{m}$, where

$$\underline{m} = \alpha \underline{E} = \alpha \underline{E}_0 e^{i(kz - \omega t)} \tag{A10}$$

In the case of a water drop we would have $\alpha = \chi_w V$. The secondary field generated by the oscillating dipole moment at distance r in a direction making angle θ with the incident wave direction is given by

$$\delta E_\perp = - \frac{\ddot{m}(t')}{rc^2} \qquad \delta E_{||} = - \frac{\ddot{m}(t') \cos\theta}{rc^2} \tag{A11}$$

where $\delta E_\perp$ and $\delta E_{||}$ are components normal and parallel to the plane containing the incident direction and the direction of r, and where $t' = t - r/c$. Thus we can write

$$\ddot{\underline{m}}(t') = \ddot{\underline{m}}(t) e^{ikr} = -\omega^2 \underline{m}(t) e^{ikr} \tag{A12}$$

In the Fresnel approximation one assumes that $\cos\theta \simeq 1$ for oscillators within the first Fresnel zone subtended by the field point ahead of the incident wave From (A10), (A11) and (A12) we find

$$\delta E_\perp = \frac{k^2 \alpha}{r} E_\perp e^{ikr} \qquad \delta E_{||} = \frac{k^2 \alpha \cos\theta}{r} E_{||} e^{ikr} \tag{A13}$$

In the case of large scattering particles the scattered field is not that of an oscillating dipole. Diffraction and geometric optics for surface reflection and refraction greatly complicate the situation Instead of (A13) we write

$$\delta E_\perp = \frac{S_1(\theta)}{ikr} E_\perp e^{ikr} \qquad \delta E_{||} = \frac{S_2(\theta)}{ikr} E_{||} e^{ikr} \tag{A14}$$

where $S_1(\theta)$ and $S_2(\theta)$ are complex scattering functions. In general these functions are evaluated from Mie theory. In the case of spheres such that $\eta \equiv ak \gg 1$, it can be shown that [15]

$$S_1(\theta) = S_2(\theta) = \eta J_1(\eta \sin\theta)/\sin\theta \tag{A15}$$

where J_1 is a Bessel function. The first dark ring of the diffraction pattern occurs at $\sin\theta = 3.83$.

Because the scattering particles are not uniformly distributed on a scale comparable to a wavelength, incoherent scatterings will be superimposed on the coherent scattering which led to a refractive index for the medium In the case of coherent scatterins we added the amplitudes of the individual Huygen-type spherical waves (e.g. by dividing the wavefront into Fresnel zones). For incoherent scatterings we add intensities. Each scattering particle extracts from the beam power equal to

$$\iint \frac{c\delta\underline{E}\times\delta\underline{B}}{4\pi}\cdot d\underline{S} = \iint \frac{c}{4\pi}\left(\frac{k^2\alpha E\sin\bar{\theta}}{r}\right)^2 r^2\sin\bar{\theta}\,d\bar{\theta}\,d\varphi$$

$$= \frac{8\pi}{3}k^4\alpha^2\left(\frac{cE^2}{4\pi}\right) = \frac{8\pi}{3}k^4\alpha^2 I \qquad \text{(B1)}$$

where $\bar{\theta}$ is the angle between the scattering direction and the dipole axis. We can relate the dipole moment of a drop $\alpha\underline{E}$ to the electric susceptibility of liquid water χ_w or to the electric susceptibility of the medium χ by

$$\alpha = V\chi_w = \chi/N. \qquad 4\pi\chi_w = n_w^2 - 1 \qquad 4\pi\chi^2 = n^2 - 1 \qquad \text{(B2)}$$

where V is the volume of a drop n_w and n are the refractive indices.

If the concentration of scatterers with radii in $a \to a + da$ is $N(a)da$, then the decrease of beam power AdI in distance dz is the power scattered out of the beam by AdzN drops, where $N = N(a)da$. Hence for the linear scattering coefficient γ_s we have

$$dI = -\gamma_s I dz \qquad \gamma_s = \frac{8\pi}{3}k^4\int\alpha^2(a)N(a)da \qquad \text{(B3)}$$

$$= \frac{2\pi^5}{\lambda^4}\int a^6 N(a)da = \frac{14.6}{\lambda^4}\int V^2 N(a)da$$

In the case when all scatterers are identical (e.g. molecules), then

$$\gamma_s = \frac{8\pi}{3}k^4\alpha^2 N = \frac{8\pi k^4\chi^2}{3N} = \frac{8\pi^3(n^2-1)^2}{3\lambda^4 N} \qquad \text{(B4)}$$

This well known relation explains why the sky is blue.

Let optics be designed to accept solid angle $\delta\Omega$ in the backward direction. Then the backscattered power picked up from each scattering particle will be

$$\frac{c}{4\pi}\delta\underline{E}_\perp\times\delta\underline{B}_\perp\cdot\underline{n}r^2\delta\Omega = \frac{c}{4\pi}\left(\frac{k^2\alpha E}{r}\right)^2 r^2\delta\Omega = k^4\alpha^2\delta\Omega I \qquad \text{(B5)}$$

From a slab of thickness dz the backscattered power picked up is

$$\frac{dP(\pi)}{P} = k^4\delta\Omega\,dz\int\alpha^2(a)N(a)da \equiv \beta(\pi)\delta\Omega dz \qquad \text{(B6)}$$

$$\beta(\pi) = \frac{3\gamma_s}{8\pi}$$

It remains to integrate over the depth of the cloud from z_1 to z_2. Assume that $\delta\Omega$ is the same for all depths. Then, if the cloud is optically deep the integration is simply accomplished by replacement of $I(z)dz$ by $\int I(z)dz = I(z)/\gamma_{ext}$. That is,

$$\frac{\delta P(\pi)}{P} = \frac{\beta(\pi)\delta\Omega}{\gamma_{ext}} \qquad \text{(B7)}$$

If one treats the drops in our laboratory clouds as dipole scatterers (the Rayleigh approximation), and if one assumes that the clouds are monodisperse with drop radius a, then from (B3) we obtain

$$\gamma_s = \frac{11.6V}{\lambda^4}\frac{\Delta\rho}{d} = \frac{48.4\,a^3\Delta\rho}{\lambda^4 d} \qquad \text{(B8)}$$

Substituting the values, $a = 1.60\,\mu m$, $\Delta\rho/d = 4 \times 10^{-6}$ and $\lambda = 10.6\,\mu m$, one finds that

$$\gamma_s = 1.57 \times 10^{-4}\ cm^{-1} \qquad \beta(\pi) = 1.87 \times 10^{-5}\ cm^{-1} \qquad \text{(B9)}$$

For our clouds $\gamma_{ext}(10.6) \simeq 4.6 \times 10^{-3}\ cm^{-1}$, so that scattering is indeed small compared to absorption, at least for the Rayleigh approximation.

Carrier et al. [16] have calculated backscattering from various types of natural cloud, and their results with the appropriate drop size distributions for the clouds are summarized in figure 13. For example, for stratus I clouds they have $N = 464\ cm^{-3}$ (as compared to our value of 3×10^2) and modal drop radius of $3.5\,\mu m$ (as compared to our $1.6\,\mu m$). Thus NV^2 for their cloud model is 0.17 its value for our laboratory clouds. Multiplying (B9) by this factor we obtain from the Rayleigh approximation $\beta(\pi) = 3.18 \times 10^{-4}\ m^{-1}$. Their calculation, based on Mie theory, is $7.42 \times 10^{-5}\ m^{-1}$. Thus Rayleigh scattering for drops of radius $3.5\,\mu m$ would overestimate the scattering coefficient by a factor of 4.3.

Regarding the power which is returned for an outgoing TEA laser pulse of 200 MW, we have the following predictions. For the laboratory clouds:

$$\delta P(\pi)/P = 4.08 \times 10^{-3}\delta\Omega = 1.63 \times 10^{-6} \qquad \text{(B10)}$$

where we use $\gamma_{ext}(10.6) = 0.46\ m^{-1}$ in formula (B7) and where we have taken $\delta\Omega = 4 \times 10^{-4}$ steradian on the grounds that our detector with sensitive area 2mm x 2mm will accept radiation from this solid angle when the radiation is focussed by a mirror of focal length 1 m (see figure 9). Thus the returned pulse should have strength 326 W which is easily detectable.

In regard to natural clouds at a range of say 3 km, the solid angle defined now by the collecting mirror of diameter 25 cm has fallen to 6×10^{-9} steradian. Assuming the cloud to be optically deep and to have extinction coefficient $0.1\ m^{-1}$ (see data of figure 13), one now expects that

$$\delta P(\pi)/P = 1.87 \times 10^{-2}\delta\Omega \simeq 10^{-10} \qquad \text{(B11)}$$

and so the returned pulse would have strength about 20 mW, again easily detectable.

References

1. P. F. Browne and P. M. Webber, Propagation of high power pulses of 10.6 μm radiation from a CO_2 TEA Laser of novel design through clouds produced by adiabatic expansion in the laboratory, Final Technical Report, European Research Office, Contract No. DAJA37-74-C-1686 (1976).

2. P.F.Browne and P.M.Webber, A compact 50-J CO_2 TEA Laser with VUV preionization and the discharge mechanism, Appl. Phys. Lett. 28, 662 (1976).

3. R. Sanders and J.E.A. Selby, Comparative measurements of the attenuation of visible and infrared Laser radiation in cloud, Technical Report of EMI Electronics Ltd., Feltham, England (1968).

4. J.E.Cole III, R.A.Dobbins and H. Semerjian, Time-resolved measurement of droplet size and concentration in cloud chambers, J. Appl. Meteorology 9, 684 (1970).

5. P.E. Dyer, D.J. James and S.A. Ramsden, Single transverse mode operation of a pulsed volume excited Atmospheric pressure CO_2 Laser using an unstable resonator, Optics Communications 5 , 236 (1972).

6. D.S. Stark, P.H. Cross and H. Foster, A compact sealed pulsed CO_2 TEA Laser, IIII J. Quantum Electronics, Q-E 11, 774 (1975).

7. R.B.Gibson, A.Javan and K. Boyer, Sealed multiatmosphere CO_2 TEA Laser: seed-gas compatible system using unheated oxide catalyst, Appl. Phys. Lett. 32, 726 (1978).

8. V.I. Little, A.C. Selden and T. Stamatakis, A gigawatt CO_2 Laser with telescopic amplifier, J. Appl. Phys. 47, 1295 (1976).

9. J. Stricker and J. Rom, A fast response thin film wattmeter for measurements of CO_2 Laser power, Rev. Sci. Instr. 43, 1168 (1972).

10. A.J.Hughes, J. O'Shaughnessy and E.R. Pike, FM-CW radar range measurement at 10 μm wavelength, IEEE J. Quantum Electronics, Q-E 8, 909 (1972).

11. G.J. Mullaney, W.H. Christiansen and D.A. Russell, Fog Dissipation using a CO_2 Laser, Appl. Phys. Lett., 13, 145 (1968).

12. P. Kafalas and A.P. Ferdinand Jr., Fog droplet vaporization and fragmentation by a 10.6 μm Laser pulse, Appl. Opt. 12, 29 (1973).

13. P. Kafalas and J. Herrmann, Dynamics and energetics of the explosive vaporization of fog droplets by a 10.6 μm Laser pulse, Appl. Opt. 12, 772 (1973).

14. M. Centeno V, The refractive index of liquid water in the near infrared spectrum, J. Opt. Soc. Am. 31, 244 (1941).

15. H.C. Van de Hulst, Light Scattering by small particles, (Wiley: New York)(1957).

16. L.W. Carrier, G.A.Cato and K.J. von Essen, The backscattering and extinction of visible and infrared radiation by selected major cloud models, Appl. Opt. 6, 1209 (1967).

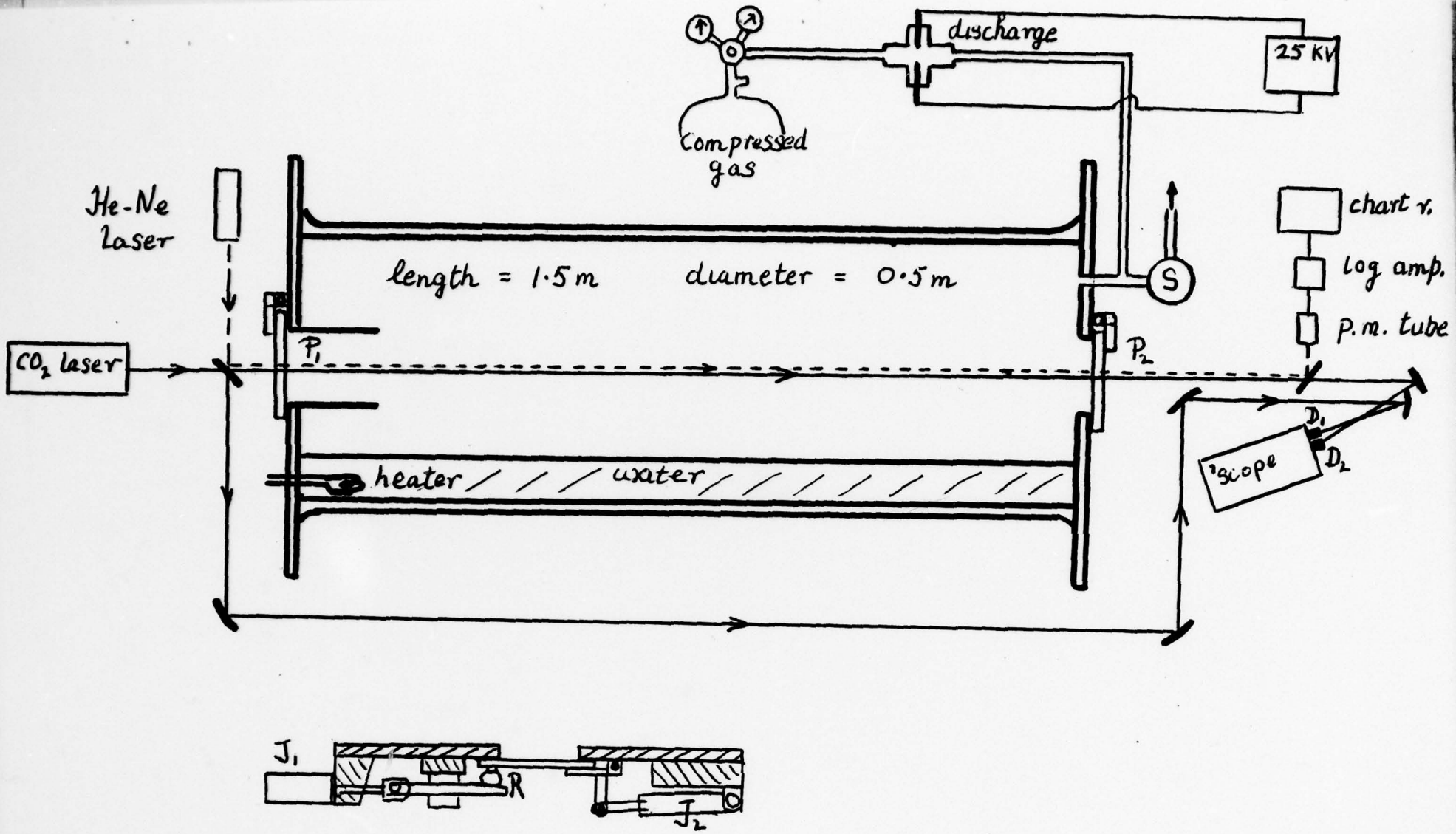

Figure 1: Expansion cloud chamber, with pneumatically controlled ports P_1 and P_2 (see insert). Following pressurization, the 1 inch solenoid valve S vents the chamber to the atmosphere. Ports P_1 and P_2 are then opened and colinear CO_2 and He-Ne laser beams are passed through the chamber. A reference CO_2 beam is deflected around the chamber. Detectors D_1 and D_2 for the CO_2 beams are mounted directly on oscilloscope in order to minimize pick-up. Insert: J_1 and J_2 are rams controlled by air pressure, and R is a roller to secure a tight seal

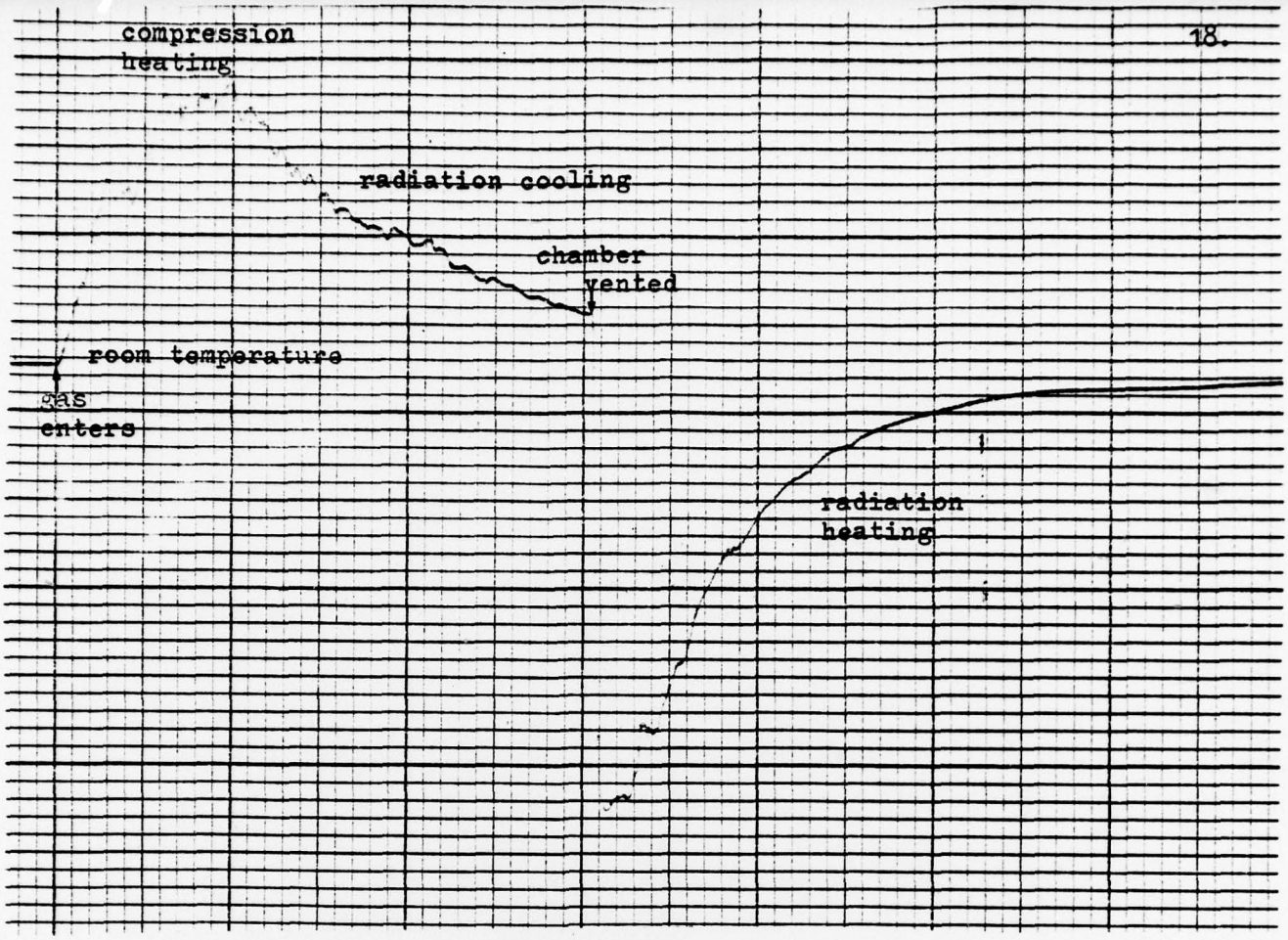

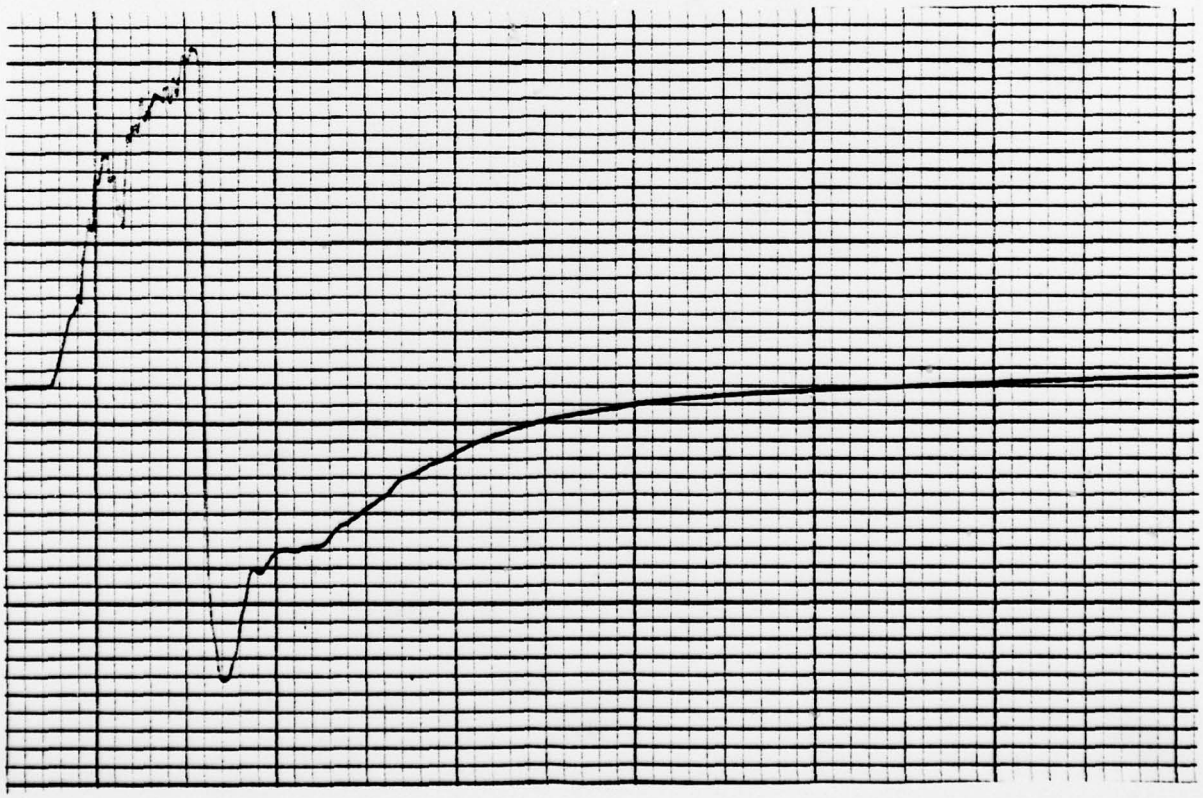

Figure 2: Temperature variation in cloud chamber as monitored by a thermocouple during two cycles of filling followed by venting. The compressed gas was allowed to cool before venting for the upper curve. The chart speed is 1" per minute in each case.

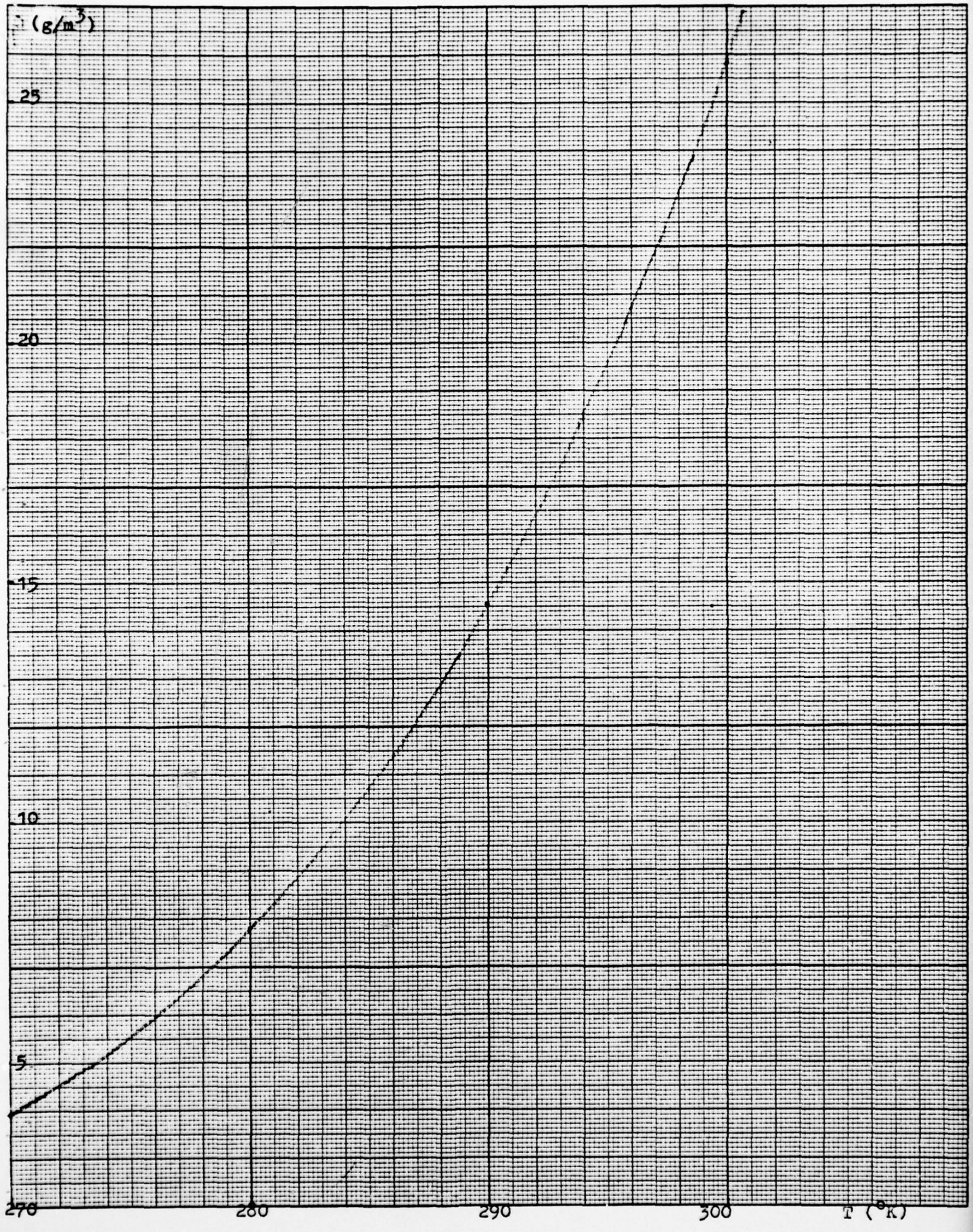

Figure 3: Water vapour content of saturated air as a function of temperature

$T_1 = 300\ ^{o}K$

Δp (psi)	$\frac{P_1}{P_2}$	$\frac{V_2}{V_1}$	ΔT (dry)	ΔT (sat.)	$\Delta \rho$ (g/m^3)
1.0	1.07	1.05	5.7	1.3	1.8
2.0	1.14	1.10	10.7	2.6	3.4
3.0	1.20	1.14	15.5	3.6	4.5
4.0	1.27	1.19	19.9	4.6	5.8
5.0	1.34	1.23	24.1	5.7	7.0
6.0	1.41	1.28	28.0	6.7	8.1
7.0	1.48	1.32	31.6	7.8	9.1
8.0	1.54	1.36	35.0	8.6	15.7

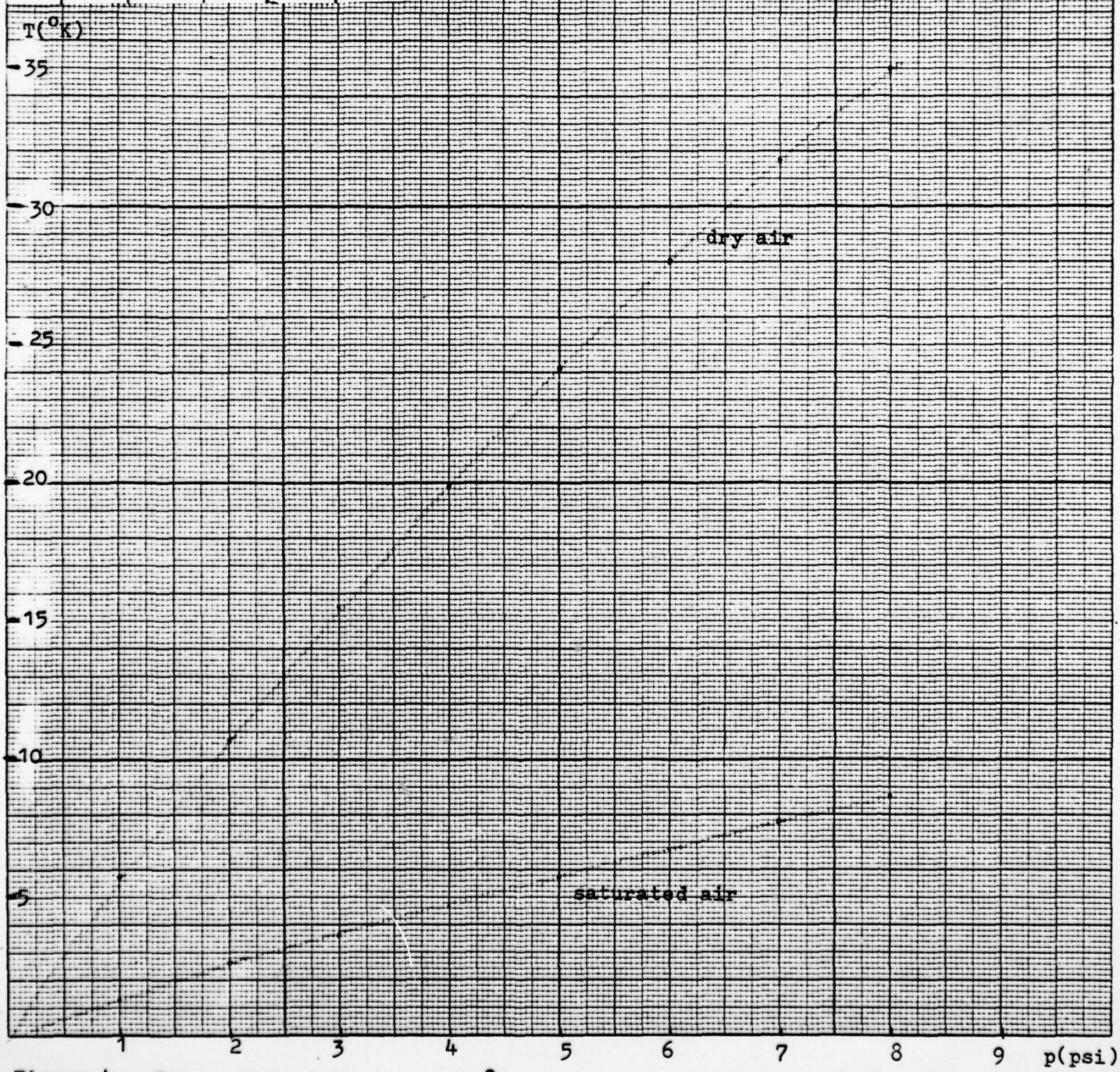

Figure 4: Temperature fall from 300 °K versus excess pressure for dry and saturated air

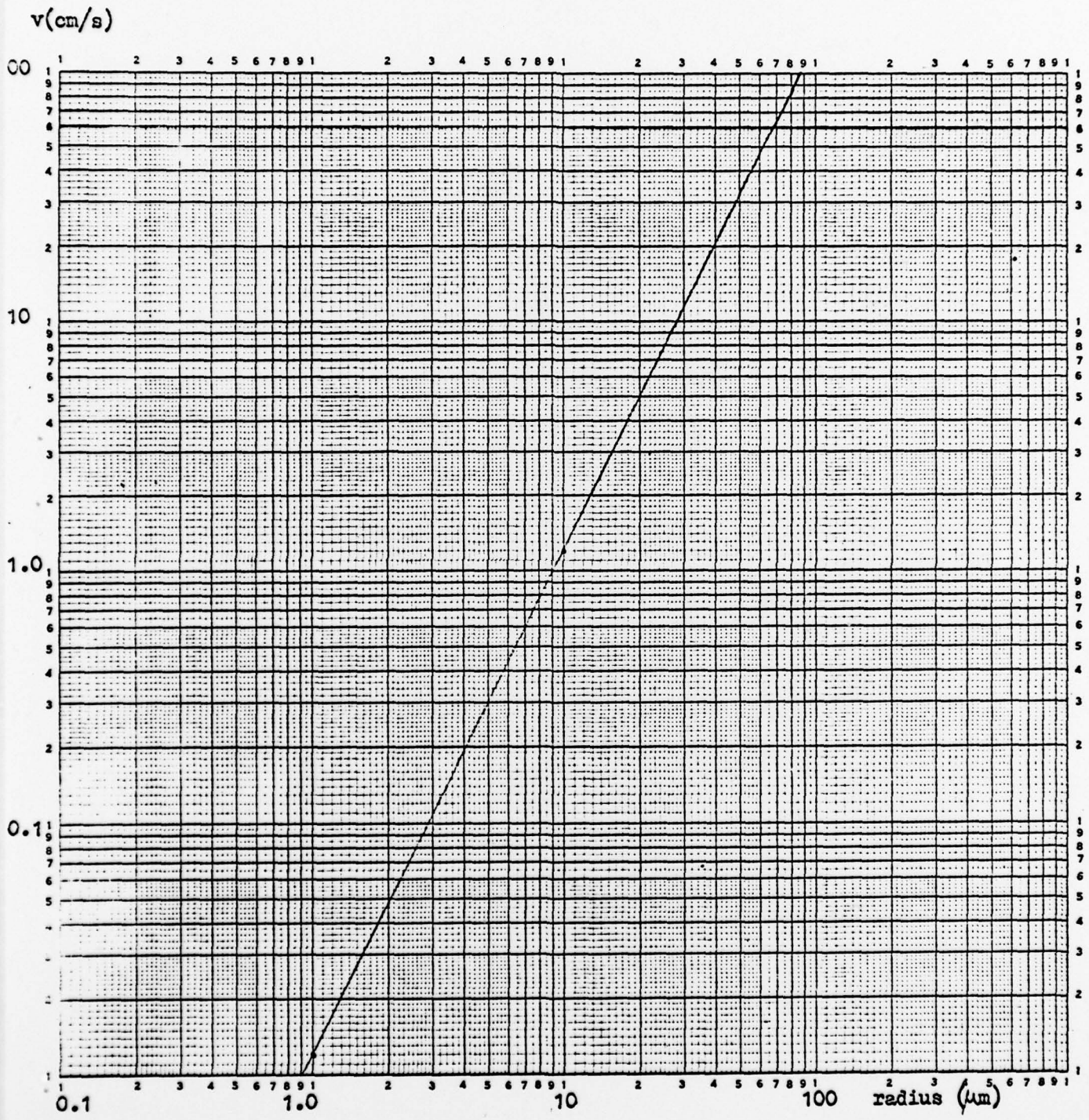

Figure 5 : Velocity of descent of drops as a function of radius according to Stokes's law.

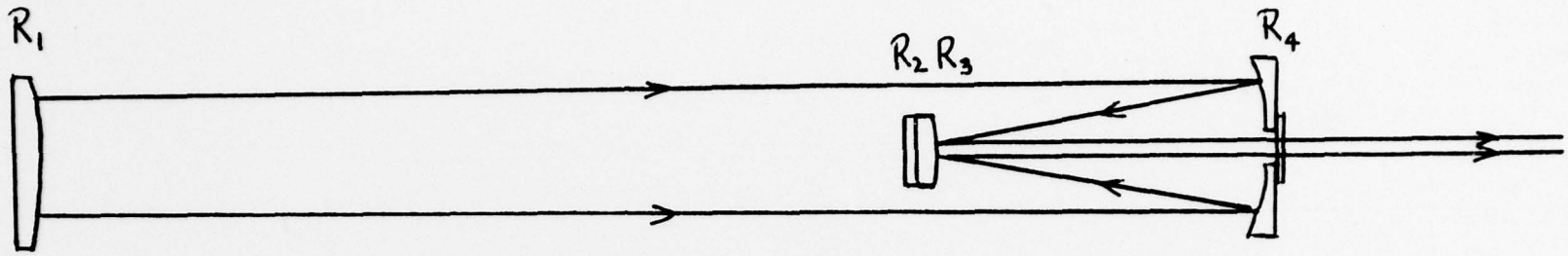

Figure 6: Large radius of curvature convex reflector R_1 and plane reflector R_2 form an unstable resonator of the type used by Dyer, James and Ramsden. Reflectors R_3 and R_4 form a Cassegrain beam reducer, whilst a Ge or KCl flat covering the central hole in R_4 serves as output window of the laser. The beam diameter is reduced from 5 cm to 1 cm .

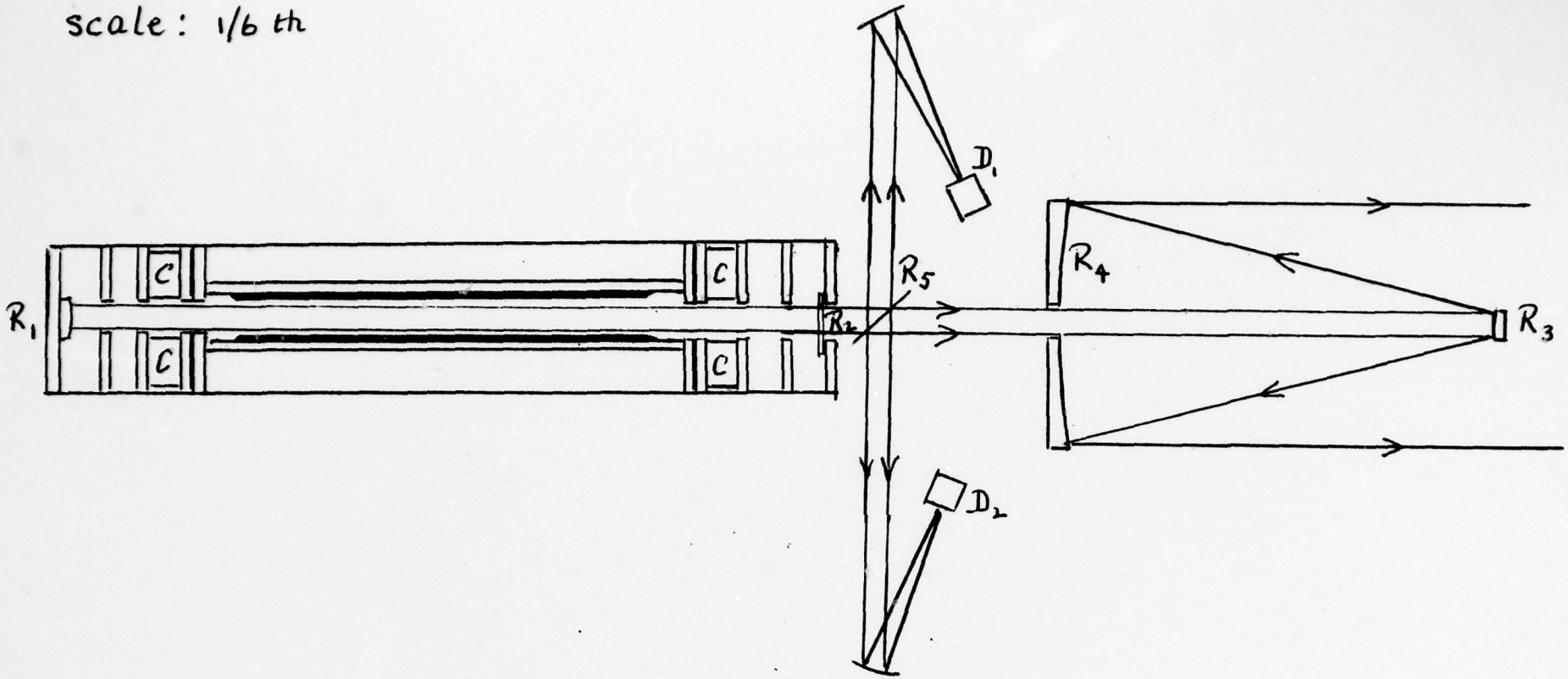

Figure 7: Portable CO_2 TEA laser and Cassegrain transmission-reception telescope with magnification 10. Output beams have diameters 1 inch and 10 inches, with angular divergences 0.5 mrad and 0.05 mrad from the laser and telescope respectively (it is assumed that the unstable resonator will give beam divergence equal to the diffraction limit for a 1 inch aperture).

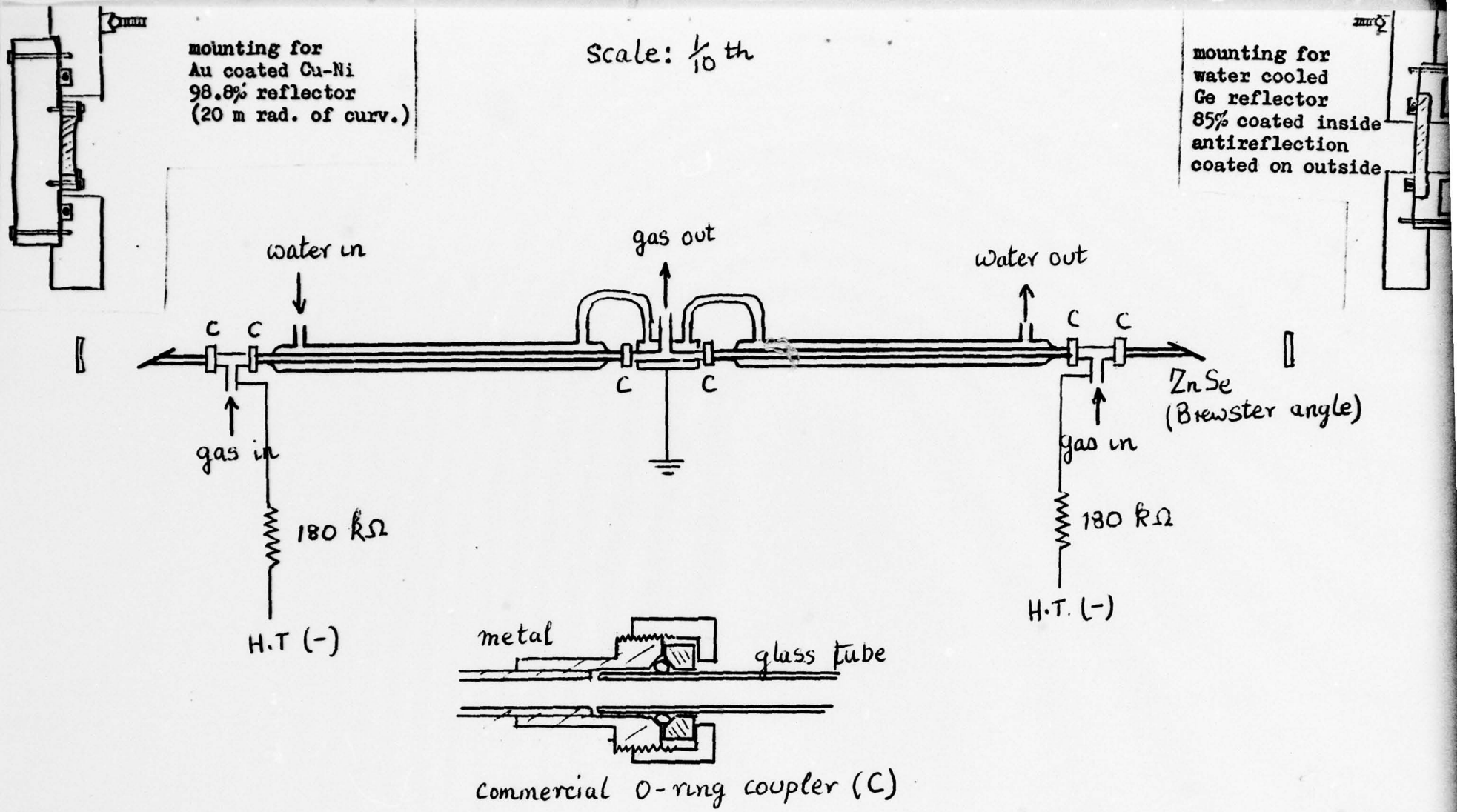

Figure 8: Construction details of CW CO_2 laser. Two pyrex glass tubes each 70 cm long and 1 cm diameter have integral cooling jackets and are coupled to metal electrodes which also serve as gas ports by O-ring couplers as shown in insert. Brewster angle ZnSe windows and external earthed and adjustable reflectors (see inserts) define the optics.

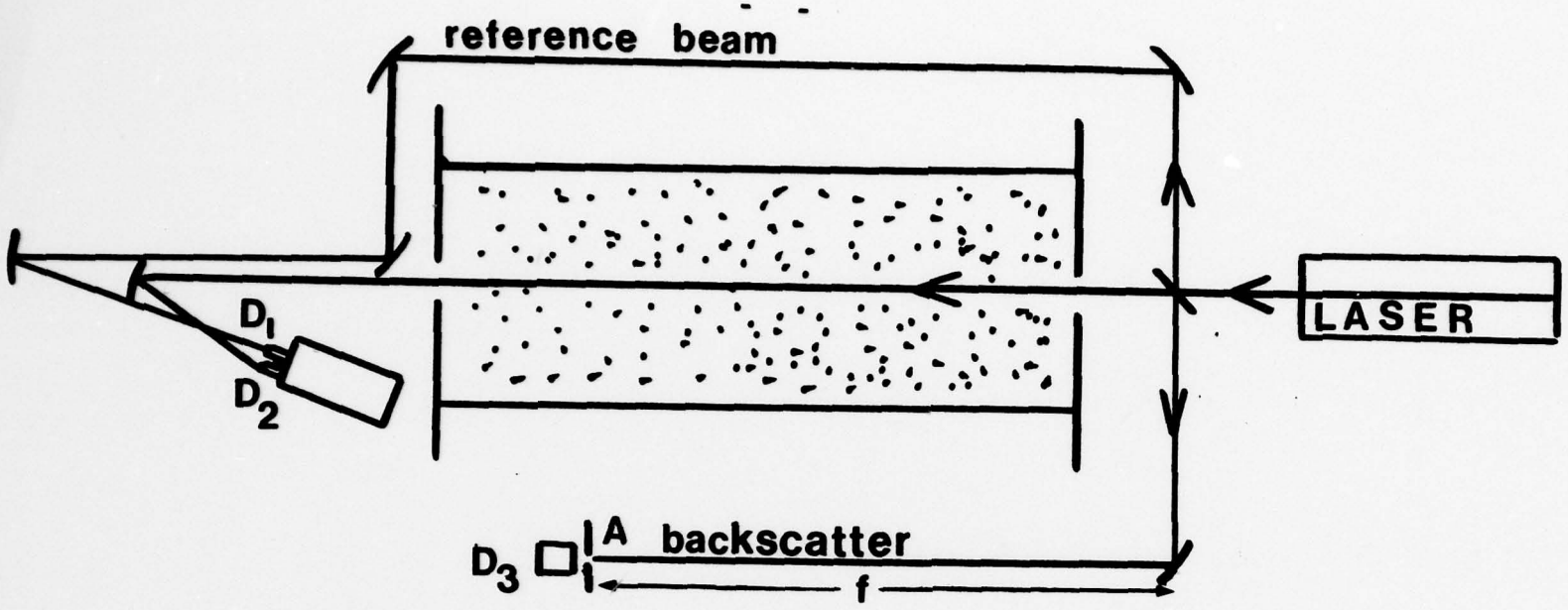

Figure 9: Experimental arrangement for measuring backscatter from laboratory clouds. The aperture A and focal length f determine the solid angle A/f from which scattered radiation is collected irrespective of drop position.

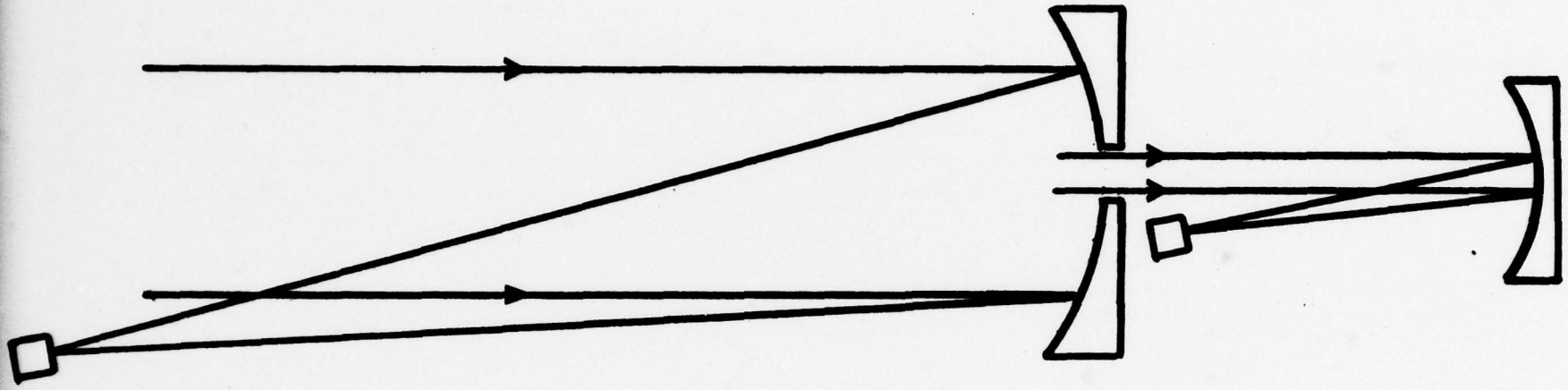

Figure 10: Measurement of beam quality n, defined by $n^2 = (P_{theory}/P_{expt})$. Here P refers to the power within a 'bucket' whose radius is defined to be $\lambda f/D$, where f is the focal length of the optics which converge the beam and D is the diameter of the laser aperture with uniform intensity and phase illumination (or the width of a Gaussian beam measured at $1/e^2$ points)

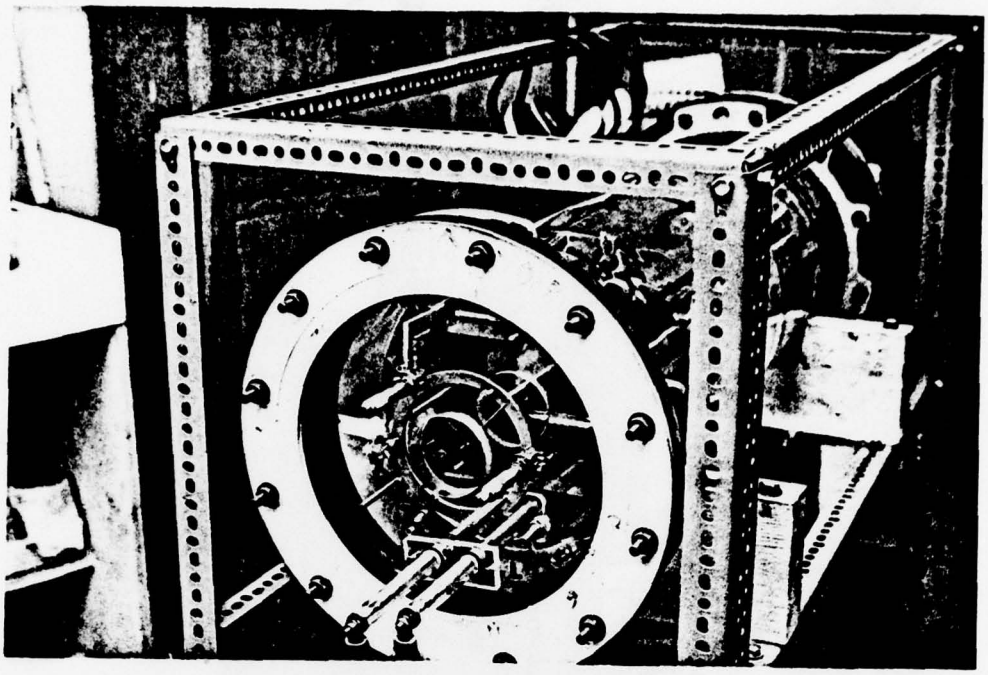

Reconstructed CO_2 TEA laser

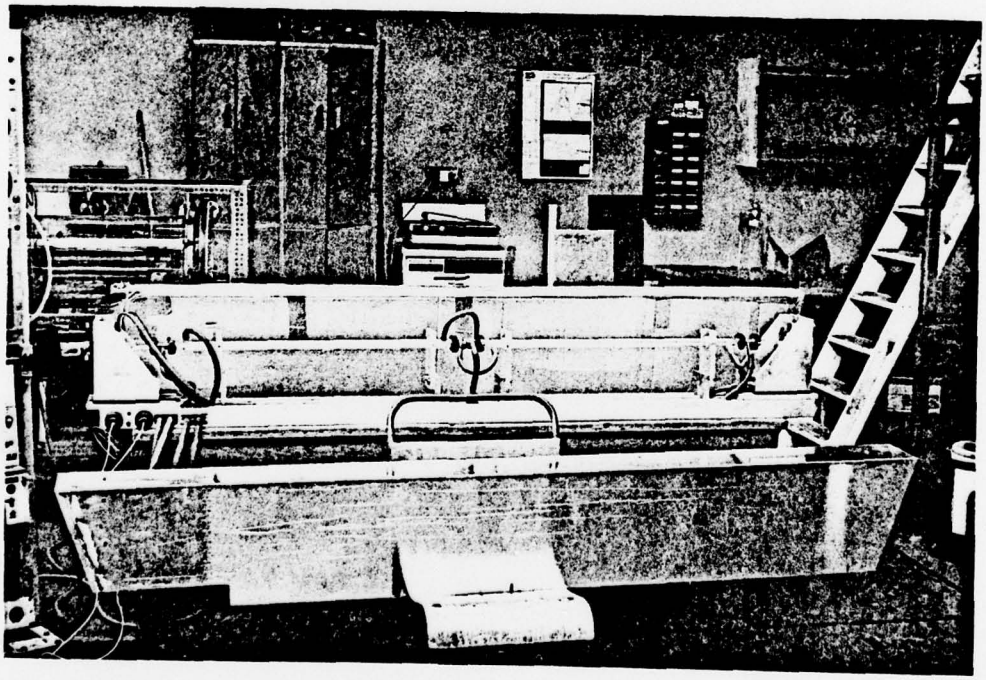

Reconstructed CW CO_2 laser

FIGURE 11: CO_2 laser systems after reconstruction

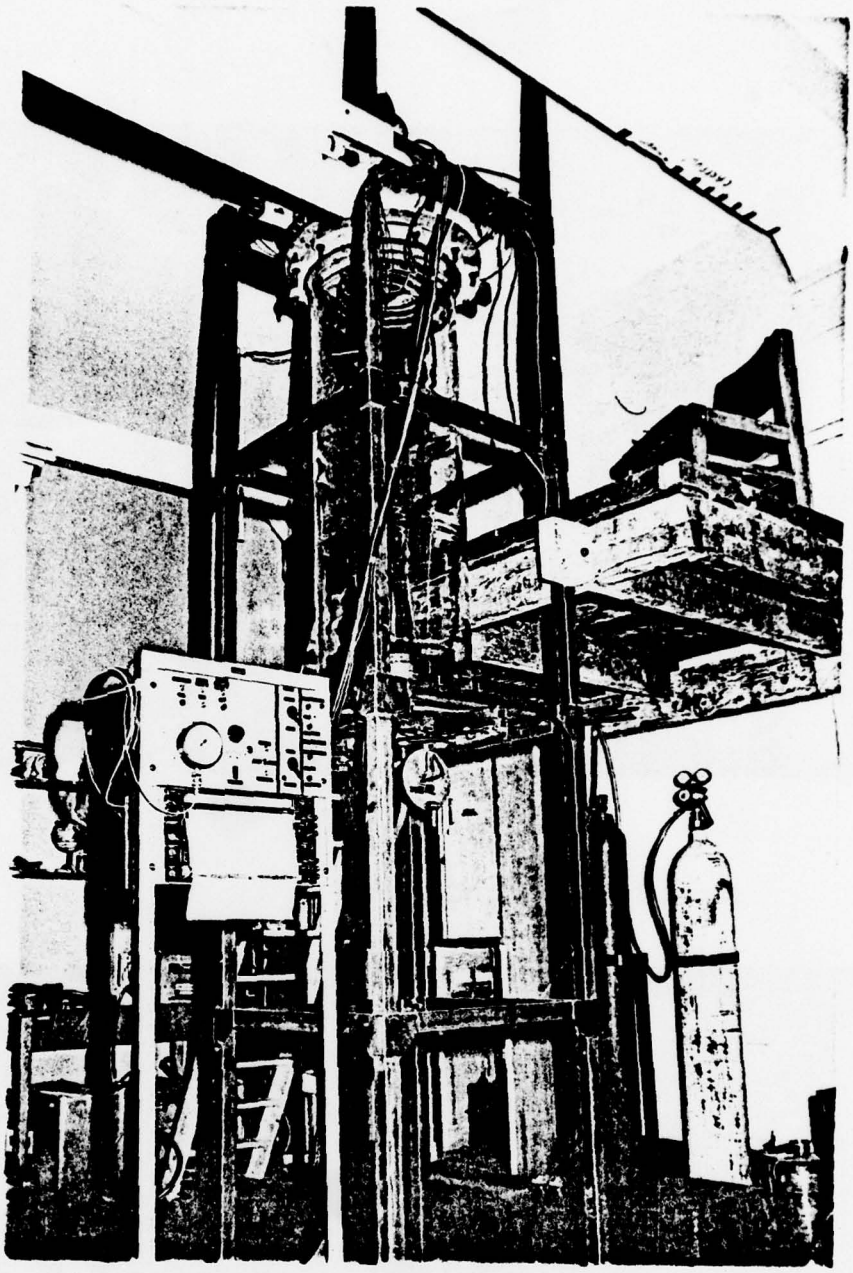

FIGURE 12: The adiabatic cloud chamber in the vertical position

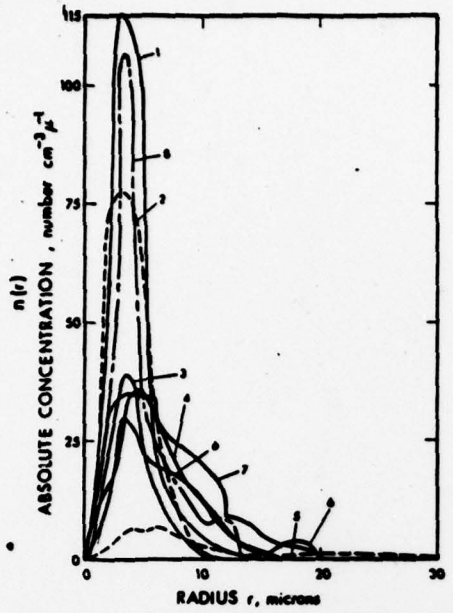

Fig. 1. Model cloud drop spectra (1) stratus I, (2) stratocumulus, (3) Fair-weather cumulus, (4) stratus II, (5) cumulonimbus, (6) cumulus congestus, (7) nimbostratus, and (8) altostratus.

Table I. Model Cloud Drop Size and Concentration

Cloud type	N^* (No./cm³)	r_{mode} (μ)	r_{min} (μ)	r_{max} (μ)	Δr (μ)
Stratus I	464	3.5	0	16.0	3.0
Altostratus	450	4.5	0	13.0	4.5
Stratocumulus	350	3.5	0	11.2	4.4
Nimbostratus	330	3.5	0	19.8	9.5
Fair-weather cumulus	300	3.5	0.5	10.0	3.0
Stratus II	260	4.5	0	20.0	5.7
Cumulus congestus	207	3.5	0	16.2	6.7
Cumulonimbus	72	5.0	0	30.0	7.0

N^* = total concentration.
r_{mode} = mode radius ≡ radius corresponding to the maximum number of droplets.
r_{min} = minimum radius.
r_{max} = maximum radius.
Δr = bandwidth of the drop-size distribution at half-value points.
μ = microns.

Table II. Summary of the Backscattering Functions and Extinction Coefficients of the Major Cloud Types

Scattering Function $\beta(\pi)$ ($m^{-1}sr^{-1}$)

Cloud type	Wavelength 0.488 μ	0.694 μ	1.06 μ	4.0 μ	10.6 μ
Nimbostratus	7.16×10^{-3}	6.03×10^{-3}	6.45×10^{-3}	3.96×10^{-3}	1.54×10^{-4}
Altostratus	6.77×10^{-3}	4.52×10^{-3}	4.99×10^{-3}	3.20×10^{-3}	1.25×10^{-4}
Stratus II	6.04×10^{-3}	4.76×10^{-3}	4.62×10^{-3}	2.87×10^{-3}	1.31×10^{-4}
Cumulus congestus	3.97×10^{-3}	3.01×10^{-3}	3.66×10^{-3}	2.43×10^{-3}	7.88×10^{-5}
Stratus I	3.13×10^{-3}	2.88×10^{-3}	3.08×10^{-3}	1.47×10^{-3}	7.42×10^{-5}
Cumulonimbus	2.40×10^{-3}	2.21×10^{-3}	2.19×10^{-3}	9.13×10^{-4}	1.16×10^{-4}
Stratocumulus	2.44×10^{-3}	1.91×10^{-3}	2.08×10^{-3}	8.91×10^{-4}	5.95×10^{-5}
Fair Wx cumulus	1.18×10^{-3}	8.68×10^{-4}	1.00×10^{-3}	4.17×10^{-4}	2.31×10^{-5}

Optical Extinction b (m^{-1})

Cloud type	Wavelength 0.488 μ	0.694 μ	1.06 μ	4.0 μ	10.6 μ
Nimbostratus	1.28×10^{-1}	1.30×10^{-1}	1.32×10^{-1}	1.47×10^{-1}	1.36×10^{-1}
Altostratus	1.08×10^{-1}	1.09×10^{-1}	1.12×10^{-1}	1.30×10^{-1}	8.39×10^{-2}
Stratus II	1.00×10^{-1}	1.01×10^{-1}	1.03×10^{-1}	1.14×10^{-1}	1.04×10^{-1}
Cumulus congestus	6.92×10^{-2}	6.98×10^{-2}	7.13×10^{-2}	8.10×10^{-2}	6.76×10^{-2}
Stratus I	6.69×10^{-2}	6.79×10^{-2}	6.97×10^{-2}	9.01×10^{-2}	4.28×10^{-2}
Cumulonimbus	4.35×10^{-2}	4.38×10^{-2}	4.44×10^{-2}	4.82×10^{-2}	5.09×10^{-2}
Stratocumulus	4.53×10^{-2}	4.60×10^{-2}	4.71×10^{-2}	5.96×10^{-2}	2.48×10^{-2}
Fair Wx cumulus	2.10×10^{-2}	2.13×10^{-2}	2.19×10^{-2}	2.76×10^{-2}	1.17×10^{-2}

Figure 13: Calculations of backscattering from various natural clouds by Carrier, Cato and von Essen (reference 16)